An unknown input observer based framework for fault and icing detection and accommodation in overactuated unmanned aerial vehicles

Andrea Cristofaro, Damiano Rotondo, Tor Arne Johansen

The use of unmanned aerial vehicles (UAVs) as support to operations in remote areas and harsh environments, such as marine operations in the Arctic, is becoming more and more crucial. These systems are expected very critical weather conditions, and for this reason they are naturally prone to the occurrence of icing. The formation of ice layers on airfoils decreases the lift and, simultaneously, increases the drag and the mass of the vehicle, thus requiring additional engine power and implying a premature stall angle. By adopting some tools from the control allocation framework, this chapter aims at presenting an unknown input observer (UIO) approach for fault and icing diagnosis and accommodation in UAVs equipped with a redundant suite of effectors and actuators. The chapter is structured as follows. At first, the UAV model and the basic setup are given, and then the fault and icing effects on the UAV dynamics are discussed. A short overview on the design of UIOs is proposed, and a main section is dedicated to present the icing diagnosis and accommodation tasks. Furthermore, by means of appropriate scheduling parameters, the UIO-based diagnosis scheme can be extended to the nonlinear aircraft dynamics by considering the framework of LPV systems. A collection of simulation examples concludes the chapter and illustrates the practical application of the proposed architecture.

1 Introduction

Detection and accommodation of ice adhesion on wings, control surfaces and sensors is a challenging and primary issue for UAVs, since the ice accretion modifies the shape of the aircraft and alters the pressure measurements, this causing adverse changes on aerodynamic forces and reducing the maneuvring capabilities. The phenomenon of icing, that can be regarded as a structural fault, is a well recognized problem in aviation research since the early 1900s [1]. Inflight icing is typically caused by the impact of supercooled water droplets (SWDs). Under certain atmospheric conditions, water droplets remain cooled and do not freeze until they reach very low temperatures; however, if a droplet impacts on the aircraft surface, it freezes immediately and accretes ice [2]. The

rate and the severity of icing are determined by several factors, such as shape and roughness of the impacting surface, vehicle speed, air temperature and relative humidity. The consequences of icing are even more severe for small unmanned aircrafts due to their simple architecture and limited payload, this making them mostly unsuitable for the typical anti-icing and de-icing devices that are used in large airplanes. Small UAVs are also more prone to icing than most other aircrafts since they often operate at low altitude where high humidity and SWDs are encountered more frequently. Larger aircrafts tend to operate at high altitude (except for take off and landing) where there are fewer risks of icing. Some advanced de-icing systems for UAVs have been proposed recently based on layers of coating material made of carbon nanotubes [3] [4]. However, since these are very power consuming, in order to guarantee the efficiency of the system it is very important to rely on fault/icing detection schemes with fast and accurate responses. On the other hand, the availability of redundant control surfaces is a key advantage toward safe aircraft maneuvering and stability in spite of icing.
UIOs [5] are a versatile and useful tool for generating robust detection filters, as they can be made insensitive to certain input space directions by assigning specific directions to the residuals as long as some structural algebraic conditions on the system are fulfilled. This is particularly interesting in connection with the control allocation framework [6, 7]. The work on UIO-based icing diagnosis has been initiated in [8] and [9], where the problem of icing detection has been addressed considering, respectively, the lateral and the longitudinal model of the vehicle. Further improvements have been obtained using multiple-models [10] and LPV methods [11] [12].

2 Vehicle model

The UAV nonlinear model consists of three equations for the airspeed components $(\tilde{u}, \tilde{v}, \tilde{w})$, which represent the velocity relative to the wind, three equations for the Euler angles $(\tilde{\phi}, \tilde{\theta}, \tilde{\psi})$, which define the attitude of the vehicle, and three equations for the angular rates $(\tilde{p}, \tilde{q}, \tilde{r})$ [13]:

$$\begin{aligned}
m\dot{\tilde{u}} &= m(\tilde{r}\tilde{v} - \tilde{q}\tilde{w} - g\sin\tilde{\theta}) + \mathcal{A}_x + \mathcal{T} \\
m\dot{\tilde{v}} &= m(\tilde{p}\tilde{w} - \tilde{r}\tilde{u} + g\cos\tilde{\theta}\sin\tilde{\phi}) + \mathcal{A}_y \\
m\dot{\tilde{w}} &= m(\tilde{q}\tilde{u} - \tilde{p}\tilde{v} + g\cos\tilde{\theta}\cos\tilde{\phi}) + \mathcal{A}_z
\end{aligned}$$

$$\begin{aligned}
\dot{\tilde{\phi}} &= \tilde{p} + \tilde{q}\sin\tilde{\phi}\tan\tilde{\theta} + \tilde{r}\cos\tilde{\phi}\tan\tilde{\theta} \\
\dot{\tilde{\theta}} &= \tilde{q}\cos\tilde{\phi} - \tilde{r}\sin\tilde{\phi} \\
\dot{\tilde{\psi}} &= \tilde{q}\sin\tilde{\phi}\sec\tilde{\theta} + \tilde{r}\cos\tilde{\phi}\sec\tilde{\theta}
\end{aligned}$$

$$\begin{aligned}
\dot{\tilde{p}} &= \Gamma_1\tilde{p}\tilde{q} - \Gamma_2\tilde{q}\tilde{r} + \mathcal{M}_p \\
\dot{\tilde{q}} &= \Gamma_5\tilde{p}\tilde{r} - \Gamma_6(\tilde{p}^2 - \tilde{r}^2) + \mathcal{M}_q \\
\dot{\tilde{r}} &= \Gamma_7\tilde{p}\tilde{q} - \Gamma_1\tilde{q}\tilde{r} + \mathcal{M}_r
\end{aligned}$$

where m is vehicle mass, g is the gravitational acceleration, $\mathcal{A}_i$ are aerodynamical forces (lift and drag), $\mathcal{T}$ is the thrust force, $\mathcal{M}_i$ are aerodynamical torques, and Γ_i are coefficients obtained as combinations of the main inertia coefficients I_{xx}, I_{yy}, I_{zz} and I_{xz}. The velocities $\tilde{u}, \tilde{v}, \tilde{w}$ are expressed in the body frame, i.e. along longitudinal, lateral and vertical body direction respectively, and they represent the aircraft speed relative to the wind.
The aerodynamical forces and torques are expressed by the quasilinear relationships

$$\begin{aligned}
\mathcal{T} &= \tfrac{\rho S_{prop} C_{prop}}{2m}\left(k_m^2 \tilde{\tau}_t - V_a^2\right) \\
\mathcal{A}_x &= \tfrac{\rho \tilde{V}_a^2 S}{2m}\left(C_X(\tilde{\alpha}) + C_{X_q}(\tilde{\alpha})\tfrac{c\tilde{q}}{2\tilde{V}_a} + C_{X_{\delta_e}}(\tilde{\alpha})\tilde{\tau}_e\right) \\
\mathcal{A}_y &= \tfrac{\rho \tilde{V}_a^2 S}{2m}\left(C_{Y_0} + C_{Y_\beta}\beta + C_{Y_p}\tfrac{b\tilde{p}}{2\tilde{V}_a} + C_{Y_r}\tfrac{b\tilde{r}}{2\tilde{V}_a} + C_{Y_{\delta_a}}\tilde{\tau}_a + C_{Y_{\delta_r}}\tilde{\tau}_r\right) \\
\mathcal{A}_z &= \tfrac{\rho \tilde{V}_a^2 S}{2m}\left(C_Z(\tilde{\alpha}) + C_{Z_q}(\tilde{\alpha})\tfrac{c\tilde{q}}{2\tilde{V}_a} + C_{Z_{\delta_e}}(\tilde{\alpha})\tilde{\tau}_e\right) \\
\mathcal{M}_p &= \tfrac{1}{2}\rho \tilde{V}_a^2 S b\left(C_{p_0} + C_{p_\beta}\tilde{\beta} + C_{p_p}\tfrac{b\tilde{p}}{2\tilde{V}_a} + C_{p_r}\tfrac{b\tilde{r}}{2\tilde{V}_a} + C_{p_{\delta_a}}\tilde{\tau}_a + C_{p_{\delta_r}}\tilde{\tau}_r\right) \\
\mathcal{M}_q &= \tfrac{\rho \tilde{V}_a^2 S c}{2I_{yy}}\left(C_{m_0} + C_{m_\alpha}\tilde{\alpha} + C_{m_q}\tfrac{c\tilde{q}}{2\tilde{V}_a} + C_{m_{\delta_e}}\tilde{\tau}_e\right) \\
\mathcal{M}_r &= \tfrac{1}{2}\rho \tilde{V}_a^2 S b\left(C_{r_0} + C_{r_\beta}\tilde{\beta} + C_{r_p}\tfrac{b\tilde{p}}{2\tilde{V}_a} + C_{r_r}\tfrac{b\tilde{r}}{2\tilde{V}_a} + C_{r_{\delta_a}}\tilde{\tau}_a + C_{r_{\delta_r}}\tilde{\tau}_r\right)
\end{aligned}$$

where ρ is the air density, S_{prop} is the area of the propeller and C_{prop} is its aerodynamical coefficient, k_m is the constant that specifies the efficiency of the motor, S is the wing surface area, m is the vehicle mass, c is the mean aerodynamic chord, and b is the wingspan of the UAV.

The overall inputs entering the system are the propeller angular speed $\tilde{\tau}_t$ (assumed to be positive) and the surface deflections $\tilde{\tau}_e, \tilde{\tau}_a$ and $\tilde{\tau}_r$ producing torques. The non-dimensional coefficients C_i are usually referred to as *stability* and *control derivatives*. Some of them are nonlinear functions of the angle-of-attack $\tilde{\alpha}$, defined as:

$$\tilde{\alpha} = \arctan\left(\tilde{u}/\tilde{w}\right)$$

according to:

$$\begin{aligned}
C_X(\tilde{\alpha}) &= (C_{L_0} + C_{L_\alpha}\tilde{\alpha})\sin\tilde{\alpha} - (C_{D_0} + C_{D_\alpha}\tilde{\alpha})\cos\tilde{\alpha} \\
C_{X_q}(\tilde{\alpha}) &= C_{L_q}\sin\tilde{\alpha} - C_{D_q}\cos\tilde{\alpha} \\
C_{X_{\delta_e}}(\tilde{\alpha}) &= C_{L_{\delta_e}}\sin\tilde{\alpha} - C_{D_{\delta_e}}\cos\tilde{\alpha} \\
C_Z(\tilde{\alpha}) &= -\left[(C_{D_0} + C_{D_\alpha}\tilde{\alpha})\sin\tilde{\alpha} + (C_{L_0} + C_{L_\alpha}\tilde{\alpha})\cos\tilde{\alpha}\right] \\
C_{Z_q}(\tilde{\alpha}) &= -\left(C_{D_q}\sin\tilde{\alpha} + C_{L_q}\cos\tilde{\alpha}\right) \\
C_{Z_{\delta_e}}(\tilde{\alpha}) &= -\left(C_{D_{\delta_e}}\sin\tilde{\alpha} + C_{L_{\delta_e}}\cos\tilde{\alpha}\right)
\end{aligned}$$

Finally, $\tilde{V}_a$ and $\tilde{\beta}$ are the total airspeed and the sideslip angle, respectively, defined as:

$$\tilde{V}_a = \sqrt{\tilde{u}^2 + \tilde{v}^2 + \tilde{w}^2}, \qquad \tilde{\beta} = \arcsin\left(\tilde{u}/\tilde{V}_a\right)$$

2.1 Linearization

The design of a complete nonlinear controller for the UAV systems is a very ambitious and challenging objective, since there are several requirements to be met and a number of different configurations and scenarios to be faced with specifically tuned performances. However, it is a common procedure to select a finite number of operating conditions, and to develop linearized control schemes for each of them: as long as the vehicle configuration lies in the hull of a given operating point, the corresponding linear controller is applied. In this regard, let us consider a suitable trim condition $x^* := (u^*, v^*, w^*, \phi^*, \theta^*, \psi^*, p^*, q^*, r^*, \tau_t^*, \tau_a^*, \tau_e^*, \tau_r^*)$ and linearize the system about such operating point. Introducing the incremental variables

$$
\begin{aligned}
&u := \tilde{u} - u^*,\ v := \tilde{v} - v^*,\ w := \tilde{w} - w^* \\
&\phi := \tilde{\phi} - \phi^*,\ \theta := \tilde{\theta} - \theta^*,\ \psi := \tilde{\psi} - \psi^* \\
&p := \tilde{p} - p^*,\ q := \tilde{q} - q^*,\ r := \tilde{r} - r^* \\
&\tau_t := \tilde{\tau}_t - \tau_t^*,\ \tau_a := \tilde{\tau}_a - \tau_a^*,\ \tau_e := \tilde{\tau}_e - \tau_e^*,\ \tau_r := \tilde{\tau}_r - \tau_r^*.
\end{aligned}
$$

one obtains a 6-DOF linear system describing the linearized coupled longitudinal/lateral dynamics of the aircraft:

$$
\dot{\mathbf{x}} = \mathbf{A}\mathbf{x} + \mathbf{B}\boldsymbol{\tau} \tag{1}
$$

with $\mathbf{x} := [u, v, w, \phi, \theta, \psi, p, q, r]^T$, $\boldsymbol{\tau} = [\tau_t, \tau_e, \tau_a, \tau_r]^T$ and plant matrices

$$
\mathbf{A} = \begin{bmatrix}
X_u & X_v & X_w & 0 & X_\theta & 0 & 0 & X_q & X_r \\
Y_u & Y_v & Y_w & Y_\phi & Y_\theta & 0 & Y_p & 0 & Y_r \\
Z_u & Z_v & Z_w & Z_\phi & Z_\theta & 0 & Z_p & Z_q & 0 \\
0 & 0 & 0 & \Phi_\phi & \Phi_\theta & 0 & \Phi_p & \Phi_q & \Phi_r \\
0 & 0 & 0 & \Theta_\phi & 0 & 0 & 0 & \Theta_q & \Theta_r \\
0 & 0 & 0 & \Psi_\phi & \Psi_\theta & 0 & 0 & \Psi_q & \Psi_r \\
L_u & L_v & L_w & 0 & 0 & 0 & L_p & L_q & L_r \\
M_u & M_v & M_w & 0 & 0 & 0 & M_p & M_q & M_r \\
N_u & N_v & N_w & 0 & 0 & 0 & N_p & N_q & N_r
\end{bmatrix}
$$

$$
\mathbf{B} = \begin{bmatrix}
X_{\tau_t} & X_{\tau_e} & 0 & 0 \\
0 & 0 & Y_{\tau_a} & Y_{\tau_r} \\
0 & Z_{\tau_e} & 0 & 0 \\
0 & 0 & 0 & 0 \\
0 & 0 & 0 & 0 \\
0 & 0 & 0 & 0 \\
0 & 0 & L_{\tau_a} & L_{\tau_r} \\
0 & M_{\tau_e} & 0 & 0 \\
0 & 0 & N_{\tau_a} & N_{\tau_r}
\end{bmatrix}
$$

The structure of such matrices is clearly provided by the linearization of the kinematic relationships, and the coefficients are essentially determined by stability and control derivatives of the vehicle.

2.2 Measured outputs

The navigation system is supposed to be equipped with a sensor suite including a pitot tube aligned with the longitudinal body axis, a GPS, an altimeter, gyroscopes and accelerometers. The following main outputs $\mathbf{y} \in \mathbb{R}^7$ are therefore considered: horizontal airspeed $y_1 = \tilde{u}$, attitude angles $(y_2, y_3, y_4) = (\tilde{\phi}, \tilde{\theta}, \tilde{\psi})$ and angular velocities $(y_5, y_6, y_7) = (\tilde{p}, \tilde{q}, \tilde{r})$; according to the linearization and the operating conditions, the output matrix $\mathring{\mathbf{C}} \in \mathbb{R}^{7\times 9}$ associated to (1) turns out to be

$$\mathring{\mathbf{C}} := \begin{bmatrix} 1 & \mathbf{0}_{1\times 2} & \mathbf{0}_{1\times 6} \\ \mathbf{0}_{6\times 1} & \mathbf{0}_{6\times 2} & \boldsymbol{I}_{6\times 6} \end{bmatrix} \tag{2}$$

In addition, the GPS and the altimeter provide position measurements $(\tilde{x}_N, \tilde{x}_E, \tilde{x}_D)$ expressed in the inertial frame; the position coordinates are assigned by the kinematic equations

$$\begin{bmatrix} \dot{\tilde{x}}_N \\ \dot{\tilde{x}}_E \\ \dot{\tilde{x}}_D \end{bmatrix} = \mathbf{R}\left(\tilde{\phi}, \tilde{\theta}, \tilde{\psi}\right) \begin{bmatrix} \tilde{u} \\ \tilde{v} \\ \tilde{w} \end{bmatrix} + \boldsymbol{\nu},$$

where the matrix $\mathbf{R}(\cdot,\cdot,\cdot)$ represents the rotation from body to inertial frame and $\boldsymbol{\nu} = [\nu_N \ \nu_E \ \nu_D]^T$ is the wind speed (expressed in the inertial frame). We notice that, whenever an accurate wind speed estimator is available [14] [15] [16], the interpolation of the estimated wind speed with the average aircraft speed, that can be computed through the GPS data, provides also a measurement of the relative velocities v, w and hence in this case one can rely on an output matrix $\bar{\mathbf{C}} \in \mathbb{R}^{9\times 9}$.

We will refer to $\mathbf{C} = \bar{\mathbf{C}}$ as to *full information case* and to $\mathbf{C} = \mathring{\mathbf{C}}$ as to *partial information case.*

2.3 Control allocation setup

We put our focus on overactuated vehicles, this being a key feature while performing tasks such as fault accommodation and control reconfiguration. The redundancy of control surfaces can be expressed by a simple, linear effector model:

$$\boldsymbol{\tau} = \mathbf{G}\boldsymbol{\delta}, \quad \boldsymbol{\delta} := \begin{bmatrix} \tau_t \\ \boldsymbol{\delta}_1 \end{bmatrix} \tag{3}$$

where $\boldsymbol{\delta}_1 \in \mathbb{R}^4$ is a vector incorporating left and right aileron deflections, and left and right rudder (or elevon) deflections:

$$\boldsymbol{\delta}_1 = \begin{bmatrix} \delta_{al} \\ \delta_{ar} \\ \delta_{rl} \\ \delta_{rr} \end{bmatrix}$$

A typical class of vehicles equipped with a surface architecture of this kind is offered, for example, by the so-called V-tail aircrafts [13]. In particular, a

pitching moment is induced when moving the ailerons jointly, while moving them alternatively produces a rolling moment. Similarly, yawing moment is induced by an alternative movement of elevons, while a joint movement produces a pitching moment. The matrix $\mathbf{G} \in \mathbb{R}^{4\times 5}$ is assigned by

$$\mathbf{G} = \begin{bmatrix} 1 & 0 & 0 & 0 & 0 \\ 0 & \epsilon & \epsilon & 1 & 1 \\ 0 & \frac{1}{2} & -\frac{1}{2} & 0 & 0 \\ 0 & 0 & 0 & 1 & -1 \end{bmatrix},$$

where the parameter $\epsilon > 0$ is inverse proportional to the distance between the aircraft center of gravity (usually assumed aligned with wings) and the tail.
Concerning the low-level control loop, the system is supposed to be controlled by an autopilot responsible to produce the desired control effect $\boldsymbol{\tau}_c$, that is typically provided by a suitable controller. The generation of the desired control effect is distributed over the redundant effectors according to (3), in particular the control allocation module is in charge to determine $\boldsymbol{\delta}_c$ such that

$$\boldsymbol{\tau}_c = \mathbf{G}\boldsymbol{\delta}_c.$$

2.4 Wind disturbance

The airspeed dynamics is affected by the wind effect, that can be expressed by the additional input

$$-\mathbf{R}\left(\tilde{\phi}, \tilde{\theta}, \tilde{\psi}\right) \dot{\boldsymbol{\nu}}$$

where $\dot{\boldsymbol{\nu}} = [\dot{\nu}_N \ \dot{\nu}_E \ \dot{\nu}_D]^T$ is the wind acceleration expressed in the inertial frame. The wind $\boldsymbol{\nu}$ is typically decomposed as the sum of a steady component (known or accurately estimated) $\boldsymbol{\nu}^*$ with $\dot{\boldsymbol{\nu}}^* = 0$ and a turbulence component $\boldsymbol{\nu}'$: this leads to an input disturbance $\boldsymbol{\xi}(t) \in \mathbb{R}^9$ given by

$$\boldsymbol{\xi}(t) = \mathbf{N}(t) \begin{bmatrix} \dot{\nu}'_N \\ \dot{\nu}'_E \\ \dot{\nu}'_D \end{bmatrix}, \ \mathbf{N}(t) := \begin{bmatrix} -\mathbf{R}\left(\tilde{\phi}, \tilde{\theta}, \tilde{\psi}\right) \\ \mathbf{0}_{6\times 3} \end{bmatrix} \tag{4}$$

Summarizing, combining (1)-(4), we have to deal with the following uncertain linear plant

$$\begin{aligned} \dot{\mathbf{x}} &= \mathbf{A}\mathbf{x} + \mathbf{B}\mathbf{G}\boldsymbol{\delta} + \mathbf{N}\dot{\boldsymbol{\nu}}' \\ \mathbf{y} &= \mathbf{C}\mathbf{x} \end{aligned} \tag{5}$$

where $\mathbf{N} = \mathbf{N}(t)$ is a time-varying input matrix. In order to model in a realistic way the wind gusts, the widely accepted Dryden wind turbulence model, also known as Dryden gusts, is used [17]. The Dryden model uses spatially varying stochastic processes to represent the components of the gusts, specifying their power spectral density.

3 Icing and fault model

The accretion of clear ice on the aircraft surfaces modifies stability and control derivatives according to the following linear model [18]

$$C_{\sharp_i}^{ice} = (1 + \eta \mathcal{K}_{\sharp_i}) C_{\sharp_i}, \quad \begin{array}{l} \sharp = X, Y, Z, L, M, N \\ i = u, v, w, p, q, r, \tau_e, \tau_a, \tau_r \end{array} \tag{6}$$

where η is the icing severity factor and the coefficient $\mathcal{K}_\sharp$ depends on aircraft specifications [18]; the clean condition corresponds to $\eta = 0$, while the all iced condition occurs for $\eta = \eta_{\max}$ [19]. Such model has been developed on the basis of real data obtained from different icing encounters [18]. The overall effect of icing can be modeled as an additive disturbance term $\eta\boldsymbol{\omega}$, where η is a scalar unknown quantity and the vector $\boldsymbol{\omega}$ is assigned by

$$\boldsymbol{\omega} = \mathbf{A}_{\mathcal{E}}\mathbf{x} + \mathbf{B}_{\mathcal{E}}\boldsymbol{\tau}$$

with

$$\mathbf{A}_{\mathcal{E}} = \begin{bmatrix} \mathcal{E}_{X_u} & \mathcal{E}_{X_v} & \mathcal{E}_{X_w} & 0 & 0 & 0 & 0 & \mathcal{E}_{X_q} & 0 \\ \mathcal{E}_{Y_u} & \mathcal{E}_{Y_v} & \mathcal{E}_{Y_w} & 0 & 0 & 0 & \mathcal{E}_{Y_p} & 0 & \mathcal{E}_{Y_r} \\ \mathcal{E}_{Z_u} & \mathcal{E}_{Z_v} & \mathcal{E}_{Z_w} & 0 & 0 & 0 & 0 & \mathcal{E}_{Z_q} & 0 \\ 0 & 0 & 0 & 0 & 0 & 0 & 0 & 0 & 0 \\ 0 & 0 & 0 & 0 & 0 & 0 & 0 & 0 & 0 \\ 0 & 0 & 0 & 0 & 0 & 0 & 0 & 0 & 0 \\ \mathcal{E}_{L_u} & \mathcal{E}_{L_v} & \mathcal{E}_{L_w} & 0 & 0 & 0 & \mathcal{E}_{L_p} & 0 & \mathcal{E}_{L_r} \\ \mathcal{E}_{M_u} & \mathcal{E}_{M_v} & \mathcal{E}_{M_w} & 0 & 0 & 0 & 0 & \mathcal{E}_{M_q} & 0 \\ \mathcal{E}_{N_u} & \mathcal{E}_{N_v} & \mathcal{E}_{N_w} & 0 & 0 & 0 & \mathcal{E}_{N_p} & 0 & \mathcal{E}_{N_r} \end{bmatrix}$$

$$\mathbf{B}_{\mathcal{E}} = \begin{bmatrix} 0 & \mathcal{E}_{X_{\tau_e}} & 0 & 0 \\ 0 & 0 & \mathcal{E}_{Y_{\tau_a}} & \mathcal{E}_{Y_{\tau_r}} \\ 0 & \mathcal{E}_{Z_{\tau_e}} & 0 & 0 \\ 0 & 0 & 0 & 0 \\ 0 & 0 & 0 & 0 \\ 0 & 0 & 0 & 0 \\ 0 & 0 & \mathcal{E}_{L_{\tau_a}} & \mathcal{E}_{L_{\tau_r}} \\ 0 & \mathcal{E}_{M_{\tau_e}} & 0 & 0 \\ 0 & 0 & \mathcal{E}_{N_{\tau_a}} & \mathcal{E}_{N_{\tau_r}} \end{bmatrix}$$

where the coefficients $\mathcal{E}_\sharp$ are obtained from $\mathcal{K}_\sharp$ and $C_\sharp$ by performing linear combinations. The icing severity factor evolves according to the law

$$\eta = f(\upsilon) \cdot \chi$$

where υ is the fraction of water freezing at a point on a surface to the water impinging on the surface,

$$\upsilon = \frac{\text{mass of water freezing}}{\text{mass of water impinging}},$$

and $\chi \geq 0$ is the accumulation parameter defined as the mass flux [20]

$$\dot{\chi} = \frac{e\lambda F_a}{\varrho c}(1 - \iota_{airfoil}), \tag{7}$$

e being the collection efficiency, λ the liquid water content, F_a is the free stream velocity, ϱ the ice density, c is the airfoil chord and $\iota_{airfoil} \in [0, 1]$ is the airfoil icing protection coefficient. Both the fraction υ and the ice density ρ depend on the air temperature and the relative humidity. In particular, when the temperature is below $-10°C$ the factor υ satisfies $\upsilon \approx 1$, this corresponding to rime ice formation; on the other hand, if the temperature is between $-10°C$ and $0°C$, glaze ice typically appears with $\upsilon < 1$. On the other hand, due to aerodynamical cooling effects, icing can also occur when the outside air temperature is close to freezing point but still warmer than $0°$. It has been observed experimentally [18] that the icing severity factor achieves its maximum $\eta_{\max}$ when the freezing fraction υ is close to the value $\upsilon_g = 0.2$, while it decreases to a steady value as υ approaches 1.
Icing can also impact on the aircraft maneuverability by decreasing the effectiveness of control surfaces. Assume that the effector position is driven by the dynamical relationships

$$\dot{\delta}_\flat = f_\flat(\delta_\flat, \gamma_\flat), \quad \flat = al, ar, rl, rr,$$

where $\gamma_\flat$ is the actuator input and the vector field $f(\cdot, \cdot)$ is supposed to be asymptotically stable for the free dynamics $\dot{\delta}_\flat = f_\flat(\delta_\flat, 0)$. The presence of ice may cause malfunctions of actuators and surface blockage; the effects can be generally modeled as the combination of loss of efficiency multiplicative factors $d_\flat(t)$ and additive factors $\varphi_\flat$:

$$\dot{\delta}_\flat = d_\flat f_\flat(\delta_\flat, \gamma_\flat) + \varphi_\flat, \quad \flat = al, ar, rl, rr \tag{8}$$

$$\begin{array}{ll} d_\flat = 1 & t \leq t_0 \\ d_\flat \in [0, 1) & t > t_0 \\ \varphi_\flat \neq 0 & t \geq t_0' \end{array} \tag{9}$$

It must be noticed that the same model catches also the effects of electrical or mechanical faults that may occur in effectors and actuators. For this reason, throughout the chapter, model (8)-(9) will be referred to as a generic effector fault.

4 Unknown Input Observer framework

The approach presented in this survey is based on unknown input observers (UIOs) [5]; the main advantage of such observers is that, if some structural conditions are met, the parameters can be designed such that the resulting estimation error is independent of some inputs of the systems, even if these are

not measured directly. In this regard, let us consider a general linear system of the form

$$\begin{cases} \dot{\mathbf{x}} = \mathbf{A}\mathbf{x} + \mathbf{B}\mathbf{v} + \mathbf{X}\mathbf{v}_{\mathbf{un}} \\ \mathbf{y} = \mathbf{C}\mathbf{x} \end{cases}$$

where $\mathbf{v}$ is the nominal input, and $\mathbf{v_{un}}$ is an unknown additional input, e.g. a disturbance. The input matrix $\mathbf{X}$ is supposed to be known. The general structure of an UIO for such linear plant is the following:

$$\begin{cases} \dot{\mathbf{z}} = \mathbf{F}\mathbf{z} + \mathbf{S}\mathbf{B}\mathbf{v} + \mathbf{K}\mathbf{y} \\ \hat{\mathbf{x}} = \mathbf{z} + \mathbf{H}\mathbf{y} \end{cases}$$

where the matrices $\mathbf{F}, \mathbf{R}, \mathbf{K}$ and $\mathbf{H}$ are design parameters. It is worth to note that, in order to achieve a correct asymptotic state estimation, the matrix $\mathbf{F}$ has to be Hurwitz, i.e. all its poles must lie in the open left half-plane. The estimation error is defined as the difference between the true state $\mathbf{x}(t)$ and the estimated state $\hat{\mathbf{x}}(t)$:

$$\boldsymbol{\epsilon}(t) = \mathbf{x}(t) - \hat{\mathbf{x}}(t).$$

Exploiting the observer structure, the dynamics of the error is ruled by the following equation

$$\begin{aligned} \dot{\boldsymbol{\epsilon}} \quad &= [(\mathbf{I_{n\times n}} - \mathbf{H}\mathbf{C})\mathbf{A} - \mathbf{K}\mathbf{C} + \mathbf{F}\mathbf{H}\mathbf{C}]\mathbf{x} - \mathbf{F}\hat{\mathbf{x}} \\ &+(\mathbf{I_{n\times n}} - \mathbf{H}\mathbf{C})\mathbf{X}\mathbf{v_{un}} + (\mathbf{I} - \mathbf{H}\mathbf{C} - \mathbf{S})\mathbf{B}\mathbf{v} \end{aligned}$$

Setting $\mathbf{K} = \mathbf{K_1} + \mathbf{K_2}$, if the following conditions are satisfied

$$\mathbf{S} = \mathbf{I_{n\times n}} - \mathbf{H}\mathbf{C} \tag{10}$$

$$\mathbf{F} = \mathbf{S}\mathbf{A} - \mathbf{K_1}\mathbf{C}, \quad \sigma(\mathbf{F}) \in \mathbb{C}^- \tag{11}$$

$$\mathbf{K_2} = \mathbf{F}\mathbf{H} \tag{12}$$

then the latter equation reduces to

$$\dot{\boldsymbol{\epsilon}} = \mathbf{F}\boldsymbol{\epsilon} + \mathbf{S}\mathbf{X}\mathbf{v_{un}}$$

where $\sigma(\cdot)$ stands for the spectrum of a matrix and the set $\mathbb{C}^-$ in the left open complex half-plane. It is worth to note that a sufficient condition for $\mathbf{F}$ to be Hurwitz is the freedom to assign the eigenvalues of the matrix $\mathbf{S}\mathbf{A} - \mathbf{K_1}\mathbf{C}$ through the feedback gain $\mathbf{K_1}$; to this purpose we give the following statement.

Theorem 4.1: *([5]) Let $\mathbf{Q} \in \mathbb{R}^{n\times\ell}$ be a matrix satisfying the following conditions*

(C1) $rank(\mathbf{Q}) = rank(\mathbf{C}\mathbf{Q})$;

(C2) the pair $(\mathbf{C}, \mathbf{A_Q})$ is detectable, where

$$\mathbf{A_Q} := \mathbf{A} - \mathbf{Q}((\mathbf{C}\mathbf{Q})^{\mathbf{T}}\mathbf{C}\mathbf{Q})^{-\mathbf{1}}(\mathbf{C}\mathbf{Q})^{\mathbf{T}}\mathbf{C}\mathbf{A}.$$

Then the matrices $\mathbf{H}, \mathbf{S}, \mathbf{F}, \mathbf{K}$ *can be found such that equalities (10)-(12) hold true together with*

$$\mathbf{SQ} = 0. \tag{13}$$

A particular solution for $\mathbf{H}$ *is given by*

$$\mathbf{H_Q} = \mathbf{Q}((\mathbf{CQ})^{\mathbf{T}}\mathbf{CQ})^{-\mathbf{1}}(\mathbf{CQ})^{\mathbf{T}}.$$

Conversely, if equalities (10)-(13) are satisfied, then $\mathbf{Q}$ *verifies* (C1) *and* (C2)*.*

The above theorem states necessary and sufficient conditions for the existence of an UIO such that (13) is satisfied. This latter condition is fundamental to make the estimation error insensitive to some of the effector/actuator faults or independent of additive uncertain inputs.
UIOs are well established and helpful tools for robust fault detection, and they have been studied already in the context of flight fault diagnosis [21] [22]. An observer satisfying property (13), is sometimes defined as a *zeroing fault input* UIO [7], and a bank of fault detection and isolation schemes can be easily designed thanks to such feature by selecting the $\mathbf{S}$ matrix in order to cancel out the whole input matrix $\mathbf{B}$ except, sequentially, its j^{th} column as j varies in $\{1, 2, ..., m\}$. By this procedure, the set of measurable signals $\{\boldsymbol{\varrho}^{(j)} = \mathbf{C}\boldsymbol{\epsilon}^{(j)}\}_{j=1}^{m}$ is provided, and the faults can be detected and isolated according to a simple logic

$$\begin{cases} ||\boldsymbol{\varrho}^{(j)}(t)|| \leq \gamma^{(j)} \Leftarrow \text{ no faults} \\ ||\boldsymbol{\varrho}^{(j)}(t)|| > \gamma^{(j)} \Rightarrow \text{ presence of faults in the } j^{th} \text{ actuator} \end{cases}$$

where $\gamma^{(j)}$ are suitable thresholds depending on measurement noise levels and other bounded perturbations. An alternative design scheme is based on UIOs with *constrained output directions* [23] [24]. Assume $m \leq p$ and consider the canonical basis of $\mathbb{R}^p$, namely $\mathbf{e}_1, ..., \mathbf{e}_p$. Since by assumption the output matrix $\mathbf{C}$ is full-rank, there exists $\boldsymbol{\Omega} \in \mathbb{R}^{n \times p}$ such that

$$\mathbf{C}\boldsymbol{\Omega} = \mathbf{I_{p \times p}} = [\mathbf{e}_1 \ \cdots \ \mathbf{e}_p].$$

The general solution of such equation is given by

$$\boldsymbol{\Omega} = \mathbf{C}^T(\mathbf{C}\mathbf{C}^T)^{-1} + [\mathbf{I_{n \times n}} - \mathbf{C}^T(\mathbf{C}\mathbf{C}^T)^{-1}\mathbf{C}]\boldsymbol{\Omega}_*, \tag{14}$$

where $\boldsymbol{\Omega}_* \in \mathbb{R}^{n \times p}$ is an arbitrary matrix. Denoting by $\boldsymbol{\Omega}_1, ..., \boldsymbol{\Omega}_p$ the columns of the matrix $\boldsymbol{\Omega}$, the basic idea of the method is to design the observer parameters in order to guarantee that, if a fault occurs in the j^{th} actuator, then the estimation error maintains the direction $\boldsymbol{\Omega}_i$ during the system evolution, this corresponding to a fixed direction $\mathbf{e}_i$ for the residual. It is worth to note that a design constraint for the achievability of this condition is that directions $\boldsymbol{\Omega}_1, ..., \boldsymbol{\Omega}_p$ need to correspond to eigenvectors of the observer matrix $\mathbf{F}$ [25].

5 Diagnosis and accommodation

5.1 Detection and Isolation in UAVs using UIOs

This section is devoted to the design of a fault diagnosis scheme able to detect the icing and to identify wether the presence of ice on a particular control surface is causing a loss of effectiveness of the surface itself, or the ice accretion on the leading edge of the wings and tail is causing a change of the airfoils aerodynamical properties. The method is to design the FD scheme based on UIOs with constrained output directions [8] [26] [9]. Referring to the effector model (3), let us consider the decomposition

$$\mathbf{G} = [\mathbf{G}_1 \ \mathbf{G_2} \ \mathbf{G_3} \ \mathbf{G_4} \ \mathbf{G_5}]$$

and set $\mathbf{W} = \mathbf{BG}$ with

$$\mathbf{W} = [\mathbf{W}_1 \ \mathbf{W_2} \ \mathbf{W_3} \ \mathbf{W_4} \ \mathbf{W_5}].$$

Consider a generic linear UIO assigned by the equations

$$\begin{aligned} \dot{\mathbf{z}} &= \mathbf{Fz} + \mathbf{SB}\boldsymbol{\tau_c} + \mathbf{Ky} \\ \hat{\mathbf{x}} &= \mathbf{z} + \mathbf{Hy} \end{aligned}$$

where $\boldsymbol{\tau}_c$ is the nominal commanded input, and assume that the observer matrices are designed such that conditions (10)-(11) are met. The matrix $\mathbf{H} \in \mathbb{R}^{9\times p}$, with either $p = 9$ or $p = 7$, is a free design parameter that can be tuned in order to assign desired directions to residuals and to decouple them from unknown input disturbances. However, due to the rank deficiency of $\mathbf{W}$, it is not possible in this cases to address a decoupled distribution of the faults effects over a set of characteristic directions in the output space and it is then required to deal with linear combinations of such directions. The two cases of full and partial information have to be treated separately.

5.1.1 Full information case

Let us consider the case $\mathbf{C} = \bar{\mathbf{C}}$ first. Referring to the wind input matrix (4), let us select three linear independent and constant vectors $\mathbf{N}_1, \mathbf{N}_2, \mathbf{N}_3 \in \mathbb{R}^9$ with

$$span\{\mathbf{N}_1, \mathbf{N}_2, \mathbf{N}_3\} = span\mathbf{N}(t) \quad \forall t \geq 0.$$

The basic idea is to make the residuals independent on the three components of the wind force, and to assign a particular output directions to each of the four input vectors corresponding to control surfaces (not including the engine throttle input vector $\mathbf{W_1}$). This is expressed by the identities

$$\bar{\mathbf{C}}(\mathbf{I} - \mathbf{H}\bar{\mathbf{C}})\mathbf{N_i} = 0, \qquad i = 1, 2, 3 \tag{15}$$

$$\bar{\mathbf{C}}(\mathbf{I} - \mathbf{H}\bar{\mathbf{C}})\mathbf{W_{i+1}} = \mathbf{e_i}, \quad i = 1, 2, 3, 4, \tag{16}$$

where $\mathbf{e_i}$ is the i^{th} vector of the standard basis in the output space $\mathbb{R}^7$. On the other hand, the four conditions (16) cannot be imposed simultaneously due

to the lack of rank of the matrix $\mathbf{G}$, and we have to limit to consider three of them. To design such matrix $\mathbf{H}$ one can proceed as follows. Select a set of three independent vectors in $\mathbb{R}^9$, namely $\{\mathbf{b_1}, \mathbf{b_2}, \mathbf{b_3}\}$, such that

$$\bar{\mathbf{C}}\mathbf{b_i} = \mathbf{e_i} \quad i = 1, 2, 3.$$

Setting $\boldsymbol{\Upsilon} = [\mathbf{0\ 0\ 0\ b_1\ b_2\ b_3}]$ and $\boldsymbol{\Lambda_{234}} = [\mathbf{N_1\ N_2\ N_3\ W_2\ W_3\ W_4}]$ with $\boldsymbol{\Upsilon}, \boldsymbol{\Lambda_{234}} \in \mathbb{R}^{9\times 6}$ a simple solution is given by

$$\mathbf{H_{234}} = (\boldsymbol{\Lambda_{234}} - \boldsymbol{\Upsilon})(\bar{\mathbf{C}}\boldsymbol{\Lambda_{234}})^{-\mathbf{L}},$$

where $(\cdot)^{-L}$ stands for the left-pseudo inverse of a matrix. Choosing a different combination, say $\boldsymbol{\Lambda_{345}} = [\mathbf{N_1\ N_2\ N_3\ W_3\ W_4\ W_5}]$, a second solution is found

$$\mathbf{H_{345}} = (\boldsymbol{\Lambda_{345}} - \boldsymbol{\Upsilon})(\bar{\mathbf{C}}\boldsymbol{\Lambda_{345}})^{-\mathbf{L}}.$$

Summarizing, we have two distinct UIOs, whose estimated states $\hat{\mathbf{x}}^{(1)}, \hat{\mathbf{x}}^{(2)}$ satisfy

$$\dot{\mathbf{x}} - \dot{\hat{\mathbf{x}}}^{(1)} = \mathbf{F}^{(1)}(\mathbf{x} - \hat{\mathbf{x}}^{(1)}) + \mathbf{S}^{(1)}(\mathbf{N}\dot{\boldsymbol{\nu}} + \mathbf{B}\mathbf{G}\tilde{\boldsymbol{\delta}} + \eta\boldsymbol{\omega}) \tag{17}$$

$$\dot{\mathbf{x}} - \dot{\hat{\mathbf{x}}}^{(2)} = \mathbf{F}^{(2)}(\mathbf{x} - \hat{\mathbf{x}}^{(2)}) + \mathbf{S}^{(2)}(\mathbf{N}\dot{\boldsymbol{\nu}} + \mathbf{B}\mathbf{G}\tilde{\boldsymbol{\delta}} + \eta\boldsymbol{\omega}) \tag{18}$$

where the matrices are defined as

$$\mathbf{F}^{(\mathrm{i})} = \mathbf{S}^{(\mathrm{i})}\mathbf{A} - \mathbf{K}_{\mathbf{1}}^{(\mathrm{i})}\bar{\mathbf{C}}, \quad i = 1, 2$$

$$\mathbf{S}^{(1)} = \mathbf{I} - \mathbf{H_{234}}\bar{\mathbf{C}}, \quad \mathbf{S}^{(2)} = \mathbf{I} - \mathbf{H_{345}}\bar{\mathbf{C}}$$

$$\mathbf{S}^{(1)}[\mathbf{W_2\ W_3\ W_4}] = \mathbf{S}^{(2)}[\mathbf{W_3\ W_4\ W_5}] = [\mathbf{b_1\ b_2\ b_3}]$$

and $\tilde{\boldsymbol{\delta}}$ is the deviation of the actual control inputs from the commanded inputs

$$\tilde{\boldsymbol{\delta}} = \boldsymbol{\delta} - \boldsymbol{\delta}_c, \text{ with } \mathbf{G}\boldsymbol{\delta_c} = \boldsymbol{\tau_c}.$$

The key point of the construction is the selection of the matrix $\mathbf{K}_{\mathbf{1}}^{(\mathrm{i})}$ $i = 1, 2$ in a way that $\mathbf{F}^{(i)}$ is Hurwitz with the triple $\{\mathbf{b_1}, \mathbf{b_2}, \mathbf{b_3}\}$ included in the set of its eigenvectors. This can be easily addressed by choosing an arbitrary Hurwitz matrix $\mathbf{M}^{(i)}$ having $\{\mathbf{b_1}, \mathbf{b_2}, \mathbf{b_3}\}$ as eigenvectors and setting

$$\mathbf{K}_{\mathbf{1}}^{(\mathrm{i})} = (\mathbf{S}^{(i)}\mathbf{A} - \mathbf{M}^{(i)})\bar{\mathbf{C}}^{-1}. \tag{19}$$

The icing identification can be performed combining the two observers, i.e. defining a suitable logic to gather information from residual directions. Let us denote by $\bar{\mathbf{\Pi}}_i$ the linear projection operator on the subspace $span\{\mathbf{e}_i\} \subset \mathbb{R}^9, i = 1, ..., 9$, e.g.

$$\bar{\mathbf{\Pi}}_1 = diag(1, 0, 0, 0, 0, 0, 0, 0, 0)$$
$$\bar{\mathbf{\Pi}}_2 = diag(0, 1, 0, 0, 0, 0, 0, 0, 0)$$
$$\vdots$$
$$\bar{\mathbf{\Pi}}_9 = diag(0, 0, 0, 0, 0, 0, 0, 0, 1).$$

Proposition 5.1: *Set* $\boldsymbol{\epsilon}^{(i)} = \bar{\mathbf{C}}(\mathbf{x} - \hat{\mathbf{x}}^{(i)})$, $i = 1, 2$. *Assume the estimator transients due to the initial conditions to be negligible, i.e.* $\boldsymbol{\epsilon}^{(i)}(0) = 0$. *Then, we can state the following decision rule.*

- $\bar{\mathbf{\Pi}}_1 \boldsymbol{\epsilon}^{(1)} = \boldsymbol{\epsilon}^{(1)} \neq 0 \Rightarrow$ *faulty effector* δ_{al}
- $\left.\begin{array}{l} \bar{\mathbf{\Pi}}_2 \boldsymbol{\epsilon}^{(1)} = \boldsymbol{\epsilon}^{(1)} \neq 0 \\ \bar{\mathbf{\Pi}}_1 \boldsymbol{\epsilon}^{(2)} = \boldsymbol{\epsilon}^{(2)} \neq 0 \end{array}\right\} \Rightarrow$ *faulty effector* δ_{ar}
- $\left.\begin{array}{l} \bar{\mathbf{\Pi}}_3 \boldsymbol{\epsilon}^{(1)} = \boldsymbol{\epsilon}^{(1)} \neq 0 \\ \bar{\mathbf{\Pi}}_2 \boldsymbol{\epsilon}^{(2)} = \boldsymbol{\epsilon}^{(2)} \neq 0 \end{array}\right\} \Rightarrow$ *faulty effector* δ_{rl}
- $\bar{\mathbf{\Pi}}_3 \boldsymbol{\epsilon}^{(2)} = \boldsymbol{\epsilon}^{(2)} \neq 0 \Rightarrow$ *faulty effector* δ_{rr}
- $\bar{\mathbf{\Pi}}_j \boldsymbol{\epsilon}^{(i)} \neq \boldsymbol{\epsilon}^{(i)}\ \forall i = 1, 2\ \forall j = 1, 2, 3 \Rightarrow$ *airfoil icing*

A formal proof of this result can be found in [27].

Remark 5.1: *The proposed decision rule can be extended to handle the case of multiple faults, i.e. the simultaneous failure of two effectors. The residuals turn out to be directed as combinations of two of the basis vectors, and hence the faulty devices can be still identified. However in this latter case, due rank deficiency, it is unlikely that exact control reconfiguration can be achieved by control allocation.*

Remark 5.2: *It is worth to note that only* 6 *of* 9 *outputs are effectively used in the proposed scheme, i.e. 3 degrees of freedom for zeroing the wind effects, and 3 degrees of freedom for assigning output directions to the columns of the matrix* $\mathbf{W}$. *Such dual redundancy may be used to enhance robustness of the algorithm in spite of sensor faults. As a matter of fact, icing may also occur on airspeed sensors, typically causing over-estimation of velocity; for this reason, in the absence of probes equipped with heating devices, it may be safer to base the icing diagnosis method on a set of* 6 *outputs only, namely* $(\phi, \theta, \psi, p, q, r)$, *in order to exclude possible biased airspeed measurements.*

5.1.2 Partial information case

In the partial information case $\mathbf{C} = \mathring{\mathbf{C}}$ we have 7 independent outputs, and hence there are 7 directions that can be freely assigned. The construction is analogous to the full information case but, since $dim(span\{\mathring{\mathbf{C}}\mathbf{N}(\mathbf{t})\}) = 1$, there is no feasible way to design the observer being decoupled from wind accelerations in the lateral and vertical directions, namely $\dot{\nu}_y^{\vdash}, \dot{\nu}_z^{\vdash}$. Similarly to the previous design procedure, we set

$$\mathbf{H_{234}} = (\mathbf{\Lambda_{234}} - \mathbf{\Upsilon})(\mathring{\mathbf{C}}\mathbf{\Lambda_{234}})^{-\mathbf{L}},$$
$$\mathbf{H_{345}} = (\mathbf{\Lambda_{345}} - \mathbf{\Upsilon})(\mathring{\mathbf{C}}\mathbf{\Lambda_{345}})^{-\mathbf{L}}$$

where the original matrices $\mathbf{\Lambda}$ and $\mathbf{\Upsilon}$ have been replaced by

$$\mathbf{\Lambda_{234}} = [\mathbf{N_1}\ \mathbf{W_2}\ \mathbf{W_3}\ \mathbf{W_4}]$$
$$\mathbf{\Lambda_{345}} = [\mathbf{N_1}\ \mathbf{W_3}\ \mathbf{W_4}\ \mathbf{W_5}]$$
$$\mathbf{\Upsilon} = [\mathbf{0}\ \mathbf{b_1}\ \mathbf{b_2}\ \mathbf{b_3}],$$

with $\mathbf{N_1} \in span\{\mathring{\mathbf{C}}\mathbf{N}(\mathbf{t})\}$. The following assumption, which is an extension of (19), guarantees that the eigenstructures of the matrices $\mathbf{F}^{(i)}$ can be assigned properly [28].

Assumption 5.1: *A matrix* $\mathbf{K_1^{(i)}}, i = 1, 2$, *can be designed such that* $\sigma(\mathbf{S}^{(i)}\mathbf{A} - \mathbf{K_1^{(i)}}\mathring{\mathbf{C}}) \in \mathbb{C}^-$ *together with*

$$\mathbf{F}^{(i)}\mathbf{b_j} = (\mathbf{S}^{(i)}\mathbf{A} - \mathbf{K_1^{(i)}}\mathring{\mathbf{C}})\mathbf{b_j} = \lambda_{\mathbf{j}}^{(i)}\mathbf{b_j} \tag{20}$$

for some $\lambda_j^{(i)} < 0$ *and* $j = 1, 2, 3$.

A sufficient condition for the existence of a gain matrix $\mathbf{K_1^{(i)}}$ with the desired properties can be found in [26].
Let us denote by $\mathring{\mathbf{\Pi}}_i$ the linear projection operator on the subspace $span\{\mathbf{e}_i\} \subset \mathbb{R}^7, i = 1, ..., 7$, e.g.

$$\mathring{\mathbf{\Pi}}_1 = diag(1, 0, 0, 0, 0, 0, 0)$$
$$\mathring{\mathbf{\Pi}}_2 = diag(0, 1, 0, 0, 0, 0, 0)$$
$$\vdots$$
$$\mathring{\mathbf{\Pi}}_7 = diag(0, 0, 0, 0, 0, 0, 1).$$

In addition we denote by $\mathring{\mathbf{\Pi}}_i^{\perp}$ the projection operator on the subspace orthogonal to $span\{\mathbf{e}_i\}$. Since in this case the wind disturbances are not completely decoupled, we need to introduce suitable thresholds in the partial information isolation scheme. Suppose that bounds on the wind accelerations are available, i.e. $|\dot{\nu}_y^{\vdash}| \leq \vartheta_y, \quad |\dot{\nu}_z^{\vdash}| \leq \vartheta_z$. Set $\boldsymbol{\vartheta} = [0\ \vartheta_y\ \vartheta_z]^T$ and

$$\boldsymbol{\mu}^{(i)}(t) = \int_0^t e^{\mathbf{F}^{(i)}(t-\varsigma)}\mathbf{S}^{(i)}\boldsymbol{\vartheta} d\varsigma,$$

the latter being an upper bound for the forced response of residuals to wind disturbances.
The following result is a generalization of the rule stated in Proposition 5.1, where the identities have been replaced by inequalities in order to take into account model uncertainties and disturbances, these being no longer decoupled from residuals in the partial information case.

Proposition 5.2: *Set* $\boldsymbol{\epsilon}^{(i)} = \mathring{\mathbf{C}}(\mathbf{x} - \hat{\mathbf{x}}^{(i)}), i = 1, 2$. *Assume the estimator transients due to the initial conditions to be negligible, i.e.* $\boldsymbol{\epsilon}^{(i)}(0) = 0$. *Then, we can state the following decision rule for* $\boldsymbol{\epsilon}^{(i)} \neq 0$*:*

- $\|\mathring{\mathbf{\Pi}}_1\epsilon^{(1)} - \epsilon^{(1)}\| \leq \|\mathring{\mathbf{\Pi}}_1^{\perp}\mu^{(1)}\| \Rightarrow$ *faulty effector* δ_{al}
- $\left.\begin{array}{l} \|\mathring{\mathbf{\Pi}}_2\epsilon^{(1)} - \epsilon^{(1)}\| \leq \|\mathring{\mathbf{\Pi}}_2^{\perp}\mu^{(1)}\| \\ \|\mathring{\mathbf{\Pi}}_1\epsilon^{(2)} - \epsilon^{(2)}\| \leq \|\mathring{\mathbf{\Pi}}_1^{\perp}\mu^{(2)}\| \end{array}\right\} \Rightarrow$ *faulty effector* δ_{ar}
- $\left.\begin{array}{l} \|\mathring{\mathbf{\Pi}}_3\epsilon^{(1)} - \epsilon^{(1)}\| \leq \|\mathring{\mathbf{\Pi}}_3^{\perp}\mu^{(1)}\| \\ \|\mathring{\mathbf{\Pi}}_2\epsilon^{(2)} - \epsilon^{(2)}\| \leq \|\mathring{\mathbf{\Pi}}_2^{\perp}\mu^{(2)}\| \end{array}\right\} \Rightarrow$ *faulty effector* δ_{rl}
- $\|\mathring{\mathbf{\Pi}}_3\epsilon^{(2)} - \epsilon^{(2)}\| \leq \|\mathring{\mathbf{\Pi}}_3^{\perp}\mu^{(2)}\| \Rightarrow$ *faulty effector* δ_{rr}
- $\|\mathring{\mathbf{\Pi}}_j\epsilon^{(i)} - \epsilon^{(i)}\| > \|\mathring{\mathbf{\Pi}}_j^{\perp}\mu^{(i)}\| \ \forall i = 1,2 \ \forall j = 1,2,3 \Rightarrow$ *airfoil icing*

Remark 5.3: *In this case, the isolation of a fault is achieved when the difference between the residual* $\epsilon^{(i)}$ *and its projection on the direction* $\mathbf{e}_j$ *remains bounded by the projection of the wind acceleration threshold* $\mu^{(i)}$ *on the orthogonal subspace* $\{\mathbf{e}_j\}^{\perp}$*. A similar logic can be adopted to handle other types of system perturbations, such as model uncertainties or measurement noise. Moreover, a frequency separation approach with the introduction of additional filters may be helpful, since wind acceleration and sensor noise are high frequency disturbances while icing is characterized by a low frequency.*

5.2 Control allocation based icing/fault accommodation

Once the icing has been detected, the control scheme is switched to some alarm mode. The alarm mode may be read as a reconfiguration in the case of effector icing [29] [7], or as the activation of an automated de-icing device in the case of accretion of ice on the leading edge of the wings [4]. Let us treat the two scenarios separately.

5.2.1 Effector icing: control reconfiguration

Suppose that one of the effectors has been identified as faulty or iced, say $\delta_{\flat^\star}$ with $\flat^\star \in \{al, ar, rl, rr\}$. Avoiding the use of the effector $\delta_{\flat^\star}$ is desirable in order to prevent loss of control, and hence the corresponding actuator input $v_{\flat^\star}$ is set to zero in (8). However, due to the presence of the factor $d_{\flat^\star}$, this does not ensure that the state of $\delta_{\flat^\star}$ converges to zero [30]; in particular, denoting by $\Psi_{\flat^\star}(t, t_d)$ the solution of the free evolution equation (8) for t larger than the fault detection time t_d, one has

$$\lim_{t\to+\infty} \Psi_{\flat^\star}(t, t_d) = \bar{\delta}_{\flat^\star} \in \mathbb{R}, \quad \delta^{\dagger}_{\flat^\star}(t) := \Psi_{\flat^\star}(t, t_d) - \bar{\delta}_{\flat^\star}.$$

With a slight abuse of notation we indicate with $\mathbf{G}_{\flat^\star}$ the column of $\mathbf{G}$ corresponding to the faulty effector, and with $\breve{\boldsymbol{\delta}} \in \mathbb{R}^4$, $\breve{\mathbf{G}}_{\flat^\star} \in \mathbb{R}^{4\times 4}$ the reduced order control input and the matrix obtained from $\mathbf{G}$ by removing the column $\mathbf{G}_{\flat^\star}$,

respectively.
The control allocation scheme is updated, and the new task is to generate a control action able to produce the desired virtual input using the safe effectors only:

$$\breve{\boldsymbol{\tau}}_c = \breve{\mathbf{G}}_{\flat^\star} \breve{\boldsymbol{\delta}},$$

where $\breve{\boldsymbol{\tau}}_c$ has also been modified in order to compensate for the torque generated by the faulty device, i.e. $\breve{\boldsymbol{\tau}}_c = \boldsymbol{\tau}_c - \mathbf{G}_{\flat^\star} \Psi_{\flat^\star}(t, t_d)$. To take into account for possible physical or operational limitations $(\delta_{al}, \delta_{ar}, \delta_{rl}, \delta_{rr}) \in \mathcal{Y}$, a direct control allocation method is proposed to generate the updated virtual input. Denoting by $\tau(\alpha)$ the diagonal matrix $\tau(\alpha) = diag(1, \alpha, \alpha, \alpha)$ with $\alpha \in [0, 1]$, the allocation reduces to the optimization problem

$$\max_{\alpha \in [0,1]} : \exists \breve{\boldsymbol{\delta}} \in \breve{\mathcal{Y}}_{\flat^\star} \text{ with } \breve{\mathbf{G}}_{\flat^\star} \breve{\boldsymbol{\delta}} = \tau(\alpha) \boldsymbol{\tau}_c$$

or, equivalently $\max_{\alpha \in [0,1]} : \breve{\boldsymbol{\delta}}_c = \breve{\mathbf{G}}_{\flat^\star}^{-1} \tau(\alpha) \boldsymbol{\tau}_c \in \breve{\mathcal{Y}}_{\flat^\star}$, where $\breve{\mathcal{Y}}_{\flat^\star}$ is the reduced-order constraint set. The advantage of direct allocation is that, even though the inputs are saturated, their joint effect has exactly the same orientation as the desired virtual input with a possible downsized magnitude, thus reducing the risk of stall angles and other hazardous conditions for aircraft stability. On the other hand, in certain operational conditions, it could be preferable to give priority to generate a particulate torque rather than the others: in this case, the direct allocation can be modified choosing independently the rescaling factors, i.e. setting $\tau = (1, \alpha_1, \alpha_2, \alpha_3)$.

We notice that, if icing occurs on several effectors, the degrees of freedom in the control allocation scheme might be insufficient to guarantee a complete reconfiguration. However, performing an estimation of the loss of efficiency (see for instance [31]) allows to compensate partially for the icing effect while keeping the faulty effectors in use.

5.2.2 Airfoil leading edge icing: automated de-icing system

If ice accretion on airfoils is detected, the automated icing protection system must be turned on, this corresponding to $\iota_{iairfoil} > 0$ in (7). The icing protection system is mainly constituted of layers of coating material, a coating temperature sensor and a microcontroller, together with a thermocouple and an electric power source [4].
The coating efficiency is regulated by the microcontroller with a PID that uses the temperature as input. The ice layers detach when the coating temperature is above $0°$: due to aerodynamic cooling effect, a safety margin is imposed to ensure complete ice melting, this corresponding to a positive reference temperature $T_\star$. In particular $\iota_{airfoil}$ is an increasing function of coating temperature T and ice thickness χ with $\iota_{airfoil}(T_\star, \chi) \geq 1$ for $\chi > 0$.

Remark 5.4: *The icing protection subsystem can also be used in anti-icing mode. Gathering atmospheric data such as relative humidity, the automated icing protection system can be turned on whenever the aircraft encounters potential icing conditions.*

6 Enhanced quasi-LPV framework

The unknown input observer framework described in Section 4 and used for detection and isolation of faults and icing in Section 5 has the limitation of considering an LTI model of the UAV, which has been obtained by linearizing the vehicle nonlinear model as described in Section 2. Therefore, the developed approach is reliable only as long as the linearized model is consistent with the nonlinear one. A way to overcome this limitation, which allows maintaining the simplicity brought by a linear structure, is to use a linear parameter varying (LPV) formulation to cope with the nonlinearities. Unlike linearization techniques, LPV methods do not involve any approximation, since they rely on an exact transformation of the original nonlinear system into a linear-like one, by incorporating all the original nonlinearities within some varying parameters that schedule the state space matrices [32]. The resulting model is referred to as *quasi-LPV*, due to the dependence of the varying parameters on endogenous signals.

6.1 Nonlinear embedding

More specifically, the UAV nonlinear model described in Section 2 can be brought to a quasi-LPV form using the nonlinear embedding in the parameters approach [33, 34]:

$$\dot{\mathbf{x}} = \mathbf{A}(\mathbf{x})\mathbf{x} + \mathbf{B}(\mathbf{x})\boldsymbol{\tau} + \mathbf{d}(\mathbf{x}) \tag{21}$$

with:

$$\mathbf{A}(\mathbf{x}) = \begin{bmatrix} X_u(\mathbf{x}) & X_v(\mathbf{x}) & X_w(\mathbf{x}) & 0 & 0 & 0 & 0 & X_q(\mathbf{x}) & X_r(\mathbf{x}) \\ Y_u(\mathbf{x}) & Y_v(\mathbf{x}) & Y_w(\mathbf{x}) & 0 & 0 & 0 & Y_p(\mathbf{x}) & 0 & Y_r(\mathbf{x}) \\ Z_u(\mathbf{x}) & Z_v(\mathbf{x}) & Z_w(\mathbf{x}) & 0 & 0 & 0 & Z_p(\mathbf{x}) & Z_q(\mathbf{x}) & 0 \\ 0 & 0 & 0 & 0 & 0 & 0 & 1 & \Phi_q(\mathbf{x}) & \Phi_r(\mathbf{x}) \\ 0 & 0 & 0 & 0 & 0 & 0 & 0 & \Theta_q(\mathbf{x}) & \Theta_r(\mathbf{x}) \\ 0 & 0 & 0 & 0 & 0 & 0 & 0 & \Psi_q(\mathbf{x}) & \Psi_r(\mathbf{x}) \\ L_u(\mathbf{x}) & L_v(\mathbf{x}) & L_w(\mathbf{x}) & 0 & 0 & 0 & L_p(\mathbf{x}) & L_q(\mathbf{x}) & L_r(\mathbf{x}) \\ M_u(\mathbf{x}) & M_v(\mathbf{x}) & M_w(\mathbf{x}) & 0 & 0 & 0 & M_p(\mathbf{x}) & M_q(\mathbf{x}) & M_r(\mathbf{x}) \\ N_u(\mathbf{x}) & N_v(\mathbf{x}) & N_w(\mathbf{x}) & 0 & 0 & 0 & N_p(\mathbf{x}) & N_q(\mathbf{x}) & N_r(\mathbf{x}) \end{bmatrix}$$

$$\mathbf{B}(\mathbf{x}) = \begin{bmatrix} X_{\tau_t} & X_{\tau_e}(\mathbf{x}) & 0 & 0 \\ 0 & 0 & Y_{\tau_a}(\mathbf{x}) & Y_{\tau_r}(\mathbf{x}) \\ 0 & Z_{\tau_e}(\mathbf{x}) & 0 & 0 \\ 0 & 0 & 0 & 0 \\ 0 & 0 & 0 & 0 \\ 0 & 0 & 0 & 0 \\ 0 & 0 & L_{\tau_a}(\mathbf{x}) & L_{\tau_r}(\mathbf{x}) \\ 0 & M_{\tau_e}(\mathbf{x}) & 0 & 0 \\ 0 & 0 & N_{\tau_a}(\mathbf{x}) & N_{\tau_r}(\mathbf{x}) \end{bmatrix}$$

$$\mathbf{d}(\mathbf{x}) = \begin{bmatrix} -g\sin\tilde{\theta} & g\cos\tilde{\theta}\sin\tilde{\phi} & g\cos\tilde{\theta}\cos\tilde{\phi} & \mathbf{0}_{1\times 6} \end{bmatrix}^T$$

where the role of the coefficients is akin to the one in the linearized model (1), although their expressions differ.

6.2 LPV unknown input observer

Taking into account the wind, the actuator faults and the icing, the quasi-LPV UAV model can be brought to the general LPV form

$$\begin{cases} \dot{\mathbf{x}} = \mathbf{A}(\boldsymbol{\vartheta})\mathbf{x} + \mathbf{B}(\boldsymbol{\vartheta})\mathbf{v} + \mathbf{X}(\boldsymbol{\vartheta})\mathbf{v_{un}} + \mathbf{d}(\boldsymbol{\vartheta}) \\ \mathbf{y} = \mathbf{C}\mathbf{x} \end{cases}$$

with notation similar to the one used in Section 4, but with the relevant property that the matrices $\mathbf{A}$, $\mathbf{B}$, $\mathbf{X}$ depend on a varying parameter vector $\boldsymbol{\vartheta}$, which is measured or estimated. It is also assumed that its derivative $\dot{\boldsymbol{\vartheta}}$ is measured or estimated.

The structure of an UIO for such LPV plant is the following

$$\begin{cases} \dot{\mathbf{z}} = \mathbf{F}(\boldsymbol{\vartheta})\mathbf{z} + \mathbf{S}(\boldsymbol{\vartheta})\mathbf{B}(\boldsymbol{\vartheta})\mathbf{v} + \mathbf{K}(\boldsymbol{\vartheta})\mathbf{y} - \dot{\mathbf{H}}(\boldsymbol{\vartheta}, \dot{\boldsymbol{\vartheta}})\mathbf{y} + \mathbf{d}(\boldsymbol{\vartheta}) - \mathbf{H}(\boldsymbol{\vartheta})\mathbf{C}\mathbf{d}(\boldsymbol{\vartheta}) \\ \hat{\mathbf{x}} = \mathbf{z} + \mathbf{H}(\boldsymbol{\vartheta})\mathbf{y} \end{cases}$$

where $\dot{\mathbf{H}}(\boldsymbol{\vartheta}, \dot{\boldsymbol{\vartheta}})$ is the time derivative of $\mathbf{H}(\boldsymbol{\vartheta})$.

Then, the dynamics of the estimation error is described by

$$\begin{aligned} \dot{\boldsymbol{\epsilon}} &= [(\mathbf{I_{n\times n}} - \mathbf{H}(\boldsymbol{\vartheta})\mathbf{C})\mathbf{A}(\boldsymbol{\vartheta}) - \mathbf{K}(\boldsymbol{\vartheta})\mathbf{C} + \mathbf{F}(\boldsymbol{\vartheta})\mathbf{H}(\boldsymbol{\vartheta})\mathbf{C}]\mathbf{x} - \mathbf{F}(\boldsymbol{\vartheta})\hat{\mathbf{x}} \\ &\quad + (\mathbf{I_{n\times n}} - \mathbf{H}(\boldsymbol{\vartheta})\mathbf{C})\mathbf{X}(\boldsymbol{\vartheta})\mathbf{v_{un}} + (\mathbf{I_{n\times n}} - \mathbf{H}(\boldsymbol{\vartheta})\mathbf{C} - \mathbf{S}(\boldsymbol{\vartheta}))\mathbf{B}(\boldsymbol{\vartheta})\mathbf{v} \end{aligned}$$

which, through the choice

$$\mathbf{S}(\boldsymbol{\vartheta}) = \mathbf{I_{n\times n}} - \mathbf{H}(\boldsymbol{\vartheta})\mathbf{C} \tag{22}$$

$$\mathbf{F}(\boldsymbol{\vartheta}) = \mathbf{S}(\boldsymbol{\vartheta})\mathbf{A}(\boldsymbol{\vartheta}) - \mathbf{K_1}(\boldsymbol{\vartheta})\mathbf{C} \tag{23}$$

$$\mathbf{K_2}(\boldsymbol{\vartheta}) = \mathbf{F}(\boldsymbol{\vartheta})\mathbf{H}(\boldsymbol{\vartheta}) \tag{24}$$

$$\mathbf{K}(\boldsymbol{\vartheta}) = \mathbf{K_1}(\boldsymbol{\vartheta}) + \mathbf{K_2}(\boldsymbol{\vartheta}) \tag{25}$$

becomes

$$\dot{\boldsymbol{\epsilon}} = \mathbf{F}(\boldsymbol{\vartheta})\boldsymbol{\epsilon} + \mathbf{S}(\boldsymbol{\vartheta})\mathbf{X}(\boldsymbol{\vartheta})\mathbf{v_{un}}$$

Notice that $\mathbf{F}(\boldsymbol{\vartheta})$ can be chosen as a constant matrix $\mathbf{F}$ through an appropriate choice of the matrix $\mathbf{K_1}(\boldsymbol{\vartheta})$, which allows assuring convergence to zero of the estimation error $\boldsymbol{\epsilon}$ with $\mathbf{v_{un}} = \mathbf{0}$ if $\sigma(\mathbf{F}) \in \mathbb{C}^-$. On the other hand, the matrix function $\mathbf{S}(\boldsymbol{\vartheta})$ can be chosen to constrain the range of $\mathbf{S}(\boldsymbol{\vartheta})\mathbf{X}(\boldsymbol{\vartheta})$, in such a way that different output directions of the residuals are assigned for the unknown inputs acting on the system, with the aim of identifying the cause for some detected system malfunctions.

6.3 Application to the UAV fault/icing diagnosis

Due to the superposition of effects and the lack of degrees of freedom in the UIO design, it is not possible to decouple completely the wind disturbance and icing effects from the actuator faults. However, it is still possible to design the UIO matrices such that a successful fault/icing diagnosis can be achieved. For the sake of simplicity, only the full information case will be detailed.

Let us notice that the following condition holds

$$\eta\boldsymbol{\omega} \in span\{\mathbf{B}(\mathbf{x}), \mathbf{e_2}, \mathbf{e_3}\} \quad \forall t \geq 0.$$

which allows us defining our target as designing the UIO matrices with the following properties

$$\mathbf{S}(\mathbf{x})[\mathbf{B}(\mathbf{x})\ \mathbf{e_2}\ \mathbf{e_3}\ \mathbf{e_4}\ \mathbf{e_5}\ \mathbf{e_6}] = \mathbf{I_{9\times 9}}$$

$$\mathbf{F}\mathbf{e_i} = \lambda_i^F \mathbf{e_i} \quad \forall i = 1, \ldots, 9$$

where $\lambda_i^F \in \mathbb{C}^-$, $i = 1, \ldots, 9$, are the desired eigenvalues of the matrix $\mathbf{F}$.

It is easy to check that the resulting matrix $\mathbf{S}(\mathbf{x})$ has the following structure:

$$\mathbf{S}\left(\mathbf{x}\right)) = \begin{pmatrix} \frac{1}{X_{\tau_t}} & 0 & 0 & 0 & 0 & 0 & 0 & s_{18}(\mathbf{x}) & 0 \\ 0 & 0 & 0 & 0 & 0 & 0 & 0 & s_{28}(\mathbf{x}) & 0 \\ 0 & 0 & 0 & 0 & 0 & 0 & s_{37}(\mathbf{x}) & 0 & s_{39}(\mathbf{x}) \\ 0 & 0 & 0 & 0 & 0 & 0 & s_{47}(\mathbf{x}) & 0 & s_{49}(\mathbf{x}) \\ 0 & 1 & 0 & 0 & 0 & 0 & s_{57}(\mathbf{x}) & 0 & s_{59}(\mathbf{x}) \\ 0 & 0 & 1 & 0 & 0 & 0 & 0 & s_{68}(\mathbf{x}) & 0 \\ 0 & 0 & 0 & 1 & 0 & 0 & 0 & 0 & 0 \\ 0 & 0 & 0 & 0 & 1 & 0 & 0 & 0 & 0 \\ 0 & 0 & 0 & 0 & 0 & 1 & 0 & 0 & 0 \end{pmatrix}$$

where the elements $s_{ij}(\mathbf{x})$ are functions of the elements appearing in $\mathbf{B}(\mathbf{x})$.

Under the assumption that at a given time either a single fault or icing could act on the system (no simultaneous multiple faults and icing), the following decision rule can be employed for faults/icing diagnosis.

Proposition 6.1: *Set $\boldsymbol{\epsilon} = \mathbf{x} - \hat{\mathbf{x}}$ and assume estimator transients due to initial conditions to be negligible, i.e. $\boldsymbol{\epsilon}(0) = 0$, and the wind to be steady, i.e. $\boldsymbol{\nu} = \boldsymbol{\nu}^*$ with $\dot{\boldsymbol{\nu}}^* = 0$. Then we can state the following decision rule.*

- $\bar{\mathbf{\Pi}}_i\boldsymbol{\epsilon} = 0 \quad \forall i = 1, \ldots, 9 \Rightarrow$ *no faults*
- $\left.\begin{array}{ll} \bar{\mathbf{\Pi}}_1\boldsymbol{\epsilon} \neq 0 & \\ \bar{\mathbf{\Pi}}_i\boldsymbol{\epsilon} = 0 & \forall i = 2, \ldots, 9 \end{array}\right\} \Rightarrow$ *faulty thrust*
- $\left.\begin{array}{ll} \bar{\mathbf{\Pi}}_2\boldsymbol{\epsilon} \neq 0 & \\ \bar{\mathbf{\Pi}}_i\boldsymbol{\epsilon} = 0 & \forall i = 1, 3, \ldots, 9 \end{array}\right\} \Rightarrow$ *faulty elevator*
- $\left.\begin{array}{ll} \bar{\mathbf{\Pi}}_3\boldsymbol{\epsilon} \neq 0 & \\ \bar{\mathbf{\Pi}}_i\boldsymbol{\epsilon} = 0 & \forall i = 1, 2, 4, \ldots, 9 \end{array}\right\} \Rightarrow$ *faulty aileron*

- $\left.\begin{array}{l} \bar{\mathbf{\Pi}}_4 \boldsymbol{\epsilon} \neq 0 \\ \bar{\mathbf{\Pi}}_i \boldsymbol{\epsilon} = 0 \quad \forall i = 1, \ldots, 3, 5, \ldots, 9 \end{array}\right\} \Rightarrow$ *faulty rudder*
- *else* $\Rightarrow$ *airfoil icing*

Remark 6.1: *A threshold-based logic similar to the one described in Section 4 should be considered due to the presence of the wind turbulence input disturbance* $\boldsymbol{\xi}(t)$ *described by* (4)*. It is worth noticing that*

$$\mathbf{S}(\mathbf{x})\mathbf{N}(t) = [\times \ 0 \ 0 \ 0 \ \times \ \times \ 0 \ 0 \ 0]$$

with $\times$ *indicating non-zero elements, which means that (at least in theory) the wind turbulence should affect only* $\bar{\mathbf{\Pi}}_i \boldsymbol{\epsilon}$*,* $i = 1, 4, 6$*. However, due to undesired effects such as presence of sensor noise and parametric uncertainties, the wind turbulence would affect the other residuals as well, although at a much smaller extent.*

7 Illustrative example: the Aerosonde UAV

The model of a typical small unmanned aircraft, the Aerosonde UAV (AAI Corporation, Textron Inc.) has been used to illustrate the use of the UIO framework for icing and fault diagnosis. A linear system describing the vehicle dynamics about the trim condition

$$\begin{gathered} u^* = 22.95 \ m/s, \ v^* = 0.5 \ m/s \ w^* = 2.3 \ m/s \\ \phi^* = 0 \ rad, \ \theta^* = 0.2 \ rad, \ \psi^* = 0 \ rad \\ p^* = 0 \ rad/s, \ q^* = 0 \ rad/s, \ r^* = 0 \ rad/s \end{gathered}$$

can be easily obtained taking a first-order approximation. Assuming the air density $\rho = 1.2682 \ Kg/m^3$, the system matrices $\mathbf{A}$, $\mathbf{B}$ can be computed using the control and stability derivatives for the Aerosonde UAV that are reported in [13]. The icing impact coefficients $\mathcal{E}$ in the matrices $A_{\mathcal{E}}$ and $B_{\mathcal{E}}$ can be estimated noticing that, in total icing conditions, the change in lift and drag coefficients has been experimentally observed to obey the rule [18]:

- 10% reduction of coefficients C_{Z_α}, $C_{Z_{\delta_e}}$, C_{m_α}, $C_{m_{\delta_e}}$, C_{p_β}, C_{p_p}, $C_{p_{\delta_a}}$
- 8% reduction of coefficients $C_{Y_{\delta_r}}$, $C_{p_{\delta_r}}$, C_{r_r}, $C_{r_{\delta_r}}$
- 20% reduction of coefficients C_{Y_β}, C_{r_β}

The system is supposed to be controlled by an autopilot and, in the considered scenario, its objective is keeping the airspeed constant while slowly changing the pitch (a ramp has been considered as reference). Wind disturbances $\boldsymbol{\nu}$ have been included in the simulations, with a maximum admissible acceleration $\|\dot{\boldsymbol{\nu}}\| \leq 8 m/s^2$.
For the sake of simplicity, only the results for the partial information case have been reported, this being the most practically significant scenario. The bank of

unknown input observers has been designed, and to show the efficiency of the methods, sensor noise has been included in the simulation study. As a matter of fact, the gain matrices $\mathbf{K_1}^{(i)}$ can be chosen as to satisfy Assumption 5.1. In the first example, a fault has been supposed to affect the left rudder δ_{rl} for $t \geq 40s$, this causing a progressive loss of efficiency of the device. Figures 1 and 2 show the behavior of residuals $\epsilon^{(1)}$, $\epsilon^{(2)}$. Despite the presence of noise and wind disturbances, in each residual a single component turns out to be distinctly affected by the control surfaces failure, i.e. direction $\mathbf{e}_3$ for residual $\epsilon^{(1)}$ and direction $\mathbf{e}_2$ for residual $\epsilon^{(2)}$: according to the decision rule, the fault can be therefore correctly identified. Control reconfiguration is activated for $t \geq 60s$ and the nominal control action is recovered, as clearly illustrated in Figure 3, where the pitch behavior is depicted. For the sake of completeness, the resulting lateral airspeed v is also reported in Figure 4, although its dynamics is only marginally affected by the fault.
The second example corresponds to incremental icing with the severity factor η slowly varying from 0 to 0.2: Figures 5 and 6 illustrate the behavior of residuals $\epsilon^{(1)}$ and $\epsilon^{(2)}$ (with partial information): each of the three components $\mathbf{e}_1, \mathbf{e}_2$ and $\mathbf{e}_3$ is significantly affected by the system perturbation, this allowing to identify the anomalous effect caused by the ice accretion on airfoils. Finally the de-icing routine has been activated, i.e. $\iota_{airfoil} > 0$ for $t \geq 120s$, and the results of icing accommodation on the longitudinal airspeed and on the pitch are shown in Figure 7 and Figure 8, respectively: the icing severity factor is reduced until a good performance of the system is recovered.

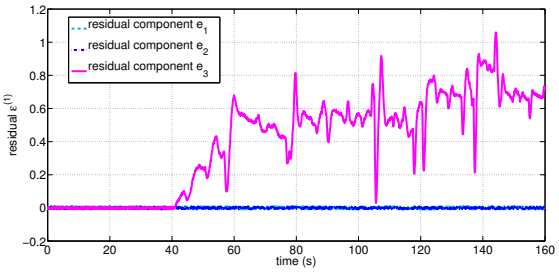

Figure 1: Faulty rudder δ_{rl}: components $\mathbf{e}_1, \mathbf{e}_2$ and $\mathbf{e}_3$ of residual $\epsilon^{(1)}$ (partial information case).

References

[1] Caliskan F, Hajiyev C. A review of in-flight detection and identification of aircraft icing and reconfigurable control. Progress in Aerospace Sciences. 2013;60:12–34.

[2] Myers TG, Hammond DW. Ice and water film growth from incoming supercooled droplets. Int Journal of Heat and Mass Transfer. 1999;42:2233–2242.

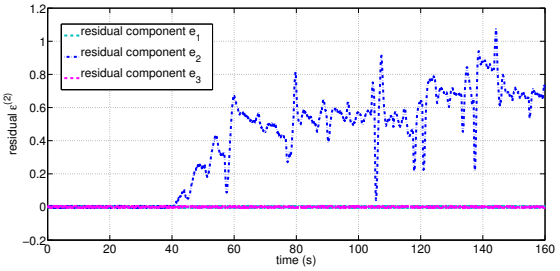

Figure 2: Faulty rudder δ_{rl}: components $\mathbf{e}_1, \mathbf{e}_2$ and $\mathbf{e}_3$ of residual $\epsilon^{(2)}$ (partial information case).

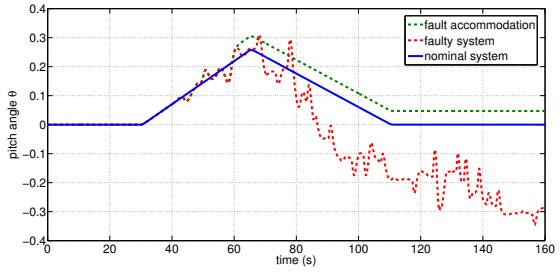

Figure 3: Pitch angle θ: reconfigured system, faulty system, nominal system

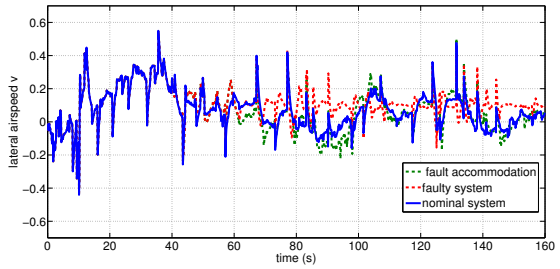

Figure 4: Lateral airspeed v: reconfigured system, faulty system, nominal system

[3] Bone S, Duff M. Carbon nanotubes to de-ice UAVs. http://13614282187/eng12/Author/data/2122docx. Technical report, 2012;.

[4] Sørensen KL, Helland AS, Johansen TA. Carbon Nanomaterial-Based Wing Temperature Control System for In-Flight Anti-Icing and De-Icing of Unmanned Aerial Vehicles. IEEE Aerospace Conference. 2015;.

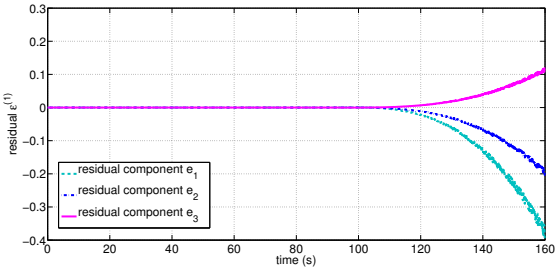

Figure 5: Incremental airfoil icing: components $\mathbf{e}_1, \mathbf{e}_2$ and $\mathbf{e}_3$ of residual $\epsilon^{(1)}$

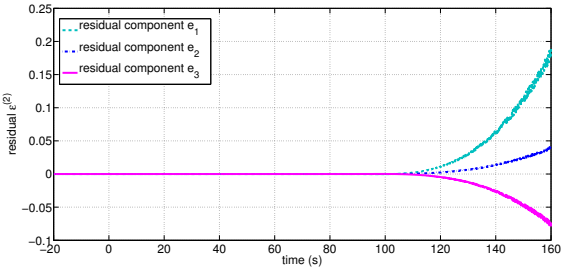

Figure 6: Incremental airfoil icing: components $\mathbf{e}_1, \mathbf{e}_2$ and $\mathbf{e}_3$ of residual $\epsilon^{(2)}$

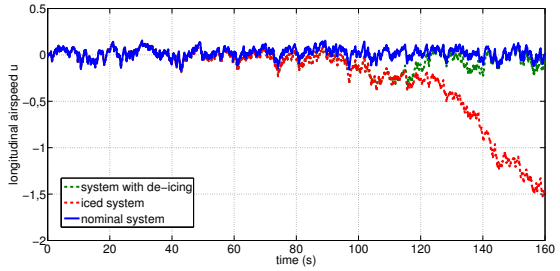

Figure 7: Horizontal airspeed u: system with ice accretion, nominal system (ice-free), activation of automated de-icing system

[5] Chen J, Patton RJ, Zhang HY. Design of unknown input observers and robust detection filters. Int J of Control. 1996;63:85–105.

[6] Johansen TA, Fossen TI. Control allocation: A survey. Automatica. 2013;49:1087–1103.

[7] Cristofaro A, Johansen TA. Fault-tolerant control allocation using Unknown Input Observers. Automatica. in press, 2014, http://dxdoiorg/101016/jautomatica201405007;.

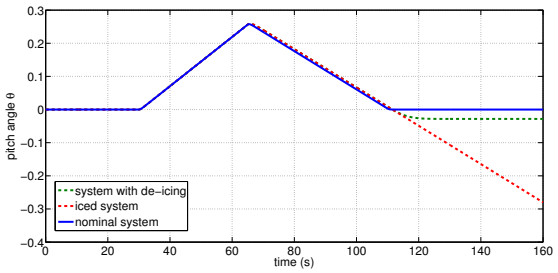

Figure 8: Pitch angle θ: system with ice accretion, nominal system (ice-free), activation of automated de-icing system

[8] Tousi M, Khorasani K. Robust observer-based fault diagnosis for an unmanned aerial vehicle. In: Systems Conference (SysCon), 2011 IEEE International; 2011. p. 428–434.

[9] Cristofaro A, Johansen TA. An unknown input observer approach to icing detection for unmanned aerial vehicles with linearized longitudinal motion. In: American Control Conference (ACC),; 2015. p. 207–213.

[10] Cristofaro A, Johansen TA, Aguiar AP. Icing Detection and Identification for Unmanned Aerial Vehicles: Multiple Model Adaptive Estimation. In: 2015 European Control Conference (ECC); 2015. p. 1645–1650.

[11] Rotondo D, Cristofaro A, Johansen TA, et al. Icing detection in unmanned aerial vehicles with longitudinal motion. In: 2015 IEEE Conference on Control Applications (CCA) - Part of the 2015 IEEE Multi-Conference on Systems and Control (MSC); 2015. p. 984–989.

[12] Seron MM, Johansen TA, De Dona' JA, et al. Detection and Estimation of Icing in Unmanned Aerial Vehicles using a Bank of Unknown Input Observers. In: Australian Control Conference (AuCC); 2015. p. 87–92.

[13] Beard RW, McLain TW. Small unmanned aircrafts - Theory and practice. Princeton University press; 2012.

[14] Langelaan JW, N, Alley, et al. Wind field estimation for small unmanned aerial vehicles. Journal of Guidance, Control, and Dynamics. 2011;34(4):1016–1030.

[15] Johansen TA, Cristofaro A, Sørensen KL, et al. On estimation of wind velocity, angle-of-attack and sideslip angle of small UAVs using standard sensors. In: Intern. Conference on Unmanned Aircraft Systems (ICUAS); 2015. p. 510–519.

[16] Wenz A, Johansen TA, Cristofaro A. Combining model-free and model-based Angle of Attack estimation for small fixed-wing UAVs using a stan-

dard sensor suite. In: Unmanned Aircraft Systems (ICUAS), 2016 International Conference on; 2016. p. 624–632.

[17] Hoblit FM. Gust loads on aircraft: concepts and applications. American Institute of Aeronautics and Astronautics; 1988.

[18] Bragg MB, Hutchinson T, Merret J, et al. Effect of ice accretion on aircraft flight dynamics. Proc 38th AIAA Aerospace Science Meeting and Exhibit. 2000;.

[19] Gent RW, Dart NP, Cansdale JT. Aircraft icing. Phil Trans of the Royal Soc of London Series A: Mathematical, Physical and Engineering Sciences. 2000;358:2873–2911.

[20] Myers TG. Extension to the Messinger model for aircraft icing. AIAA journal. 2001;39(2):211–218.

[21] Hajiyev C, Caliskan F. Fault diagnosis and reconfiguration in flight control systems. Springer Science & Business Media; 2003.

[22] Wang D, Lum KY. Adaptive unknown input observer approach for aircraft actuator fault detection and isolation. Int J of Adaptive Control and Signal Processing. 2007;21(1):31–48.

[23] Massoumnia MA. A geometric approach to the synthesis of failure detection filters. IEEE Transactions on automatic control. 1986;31(9):839–846.

[24] White J, Speyer J. Detection filter design: Spectral theory and algorithms. IEEE Transactions on Automatic Control. 1987;32(7):593–603.

[25] Park J, Rizzoni G. An eigenstructure assignment algorithm for the design of fault detection filters. IEEE Transactions on Automatic Control. 1994;39(7):1521–1524.

[26] Cristofaro A, Johansen TA. Fault-tolerant control allocation: An Unknown Input Observer based approach with constrained output fault directions. Proc 52nd IEEE Conf on Decision and Control. 2013;p. 3818–3824.

[27] Cristofaro A, Johansen TA. An unknown input observer based control allocation scheme for icing diagnosis and accommodation in overactuated UAVs. In: 2016 European Control Conference (ECC); 2016. p. 2171–2178.

[28] Park J, Rizzoni G. An eigenstructure assignment algorithm for the design of fault detection filters. IEEE Transactions on Automatic Control. 1994;39(7):1521–1524.

[29] Zhang Y, Suresh S, Jiang B, et al. Reconfigurable control allocation against aircraft control effector failures. Proc 16th IEEE Conf on Control Applications. 2007;p. 1197–1202.

[30] Cristofaro A, Johansen TA. Fault-tolerant control allocation with actuator dynamics: finite-time control reconfiguration. Proc 53rd IEEE Conf on Decision and Control. 2014;p. 4971–4976.

[31] Cristofaro A, Polycarpou MM, Johansen TA. Fault diagnosis and fault-tolerant control allocation for a class of nonlinear systems with redundant inputs. In: Proc. 54th IEEE Conf. on Decision and Control; 2015. p. 5117–5123.

[32] Shamma JS. An overview of LPV systems. In: Mohammadpour J, Scherer C, editors. Control of Linear Parameter Varying Systems with Applications. Springer; 2012. .

[33] Kwiatkowski A, Boll MT, Werner H. Automated Generation and Assessment of Affine LPV Models. In: Proceedings of the 45th IEEE Conference on Decision and Control; 2006. p. 6690–6695.

[34] Rotondo D, Puig V, Nejjari F, et al. Automated generation and comparison of Takagi-Sugeno and polytopic quasi-LPV models. Fuzzy Sets and Systems. 2015;277:44–64.